Coulomb-corrected quantum-trajectories method for recollision-impact double ionization in an intense laser field

Yuxing Bai,[1,2] Xiaolei Hao,[1,*] Weidong Li,[3] Weifeng Yang,[4,†] and Jing Chen[3,5,‡]

[1]*Institute of Theoretical Physics and Department of Physics, State Key Laboratory of Quantum Optics and Quantum Optics Devices, Collaborative Innovation Center of Extreme Optics, Shanxi University, Taiyuan 030006, China*

[2]*Department of Computer Science and Technology, Taiyuan University, Taiyuan 237016, China*

[3]*Shenzhen Key Laboratory of Ultraintense Laser and Advanced Material Technology, Center for Advanced Material Diagnostic Technology, and College of Engineering Physics, Shenzhen Technology University, Shenzhen 518118, China*

[4]*Department of Physics, School of Science, Hainan University, Haikou 570228, China*

[5]*Institute of Applied Physics and Computational Mathematics, P. O. Box 8009, Beijing 100088, China*

(Received 26 June 2023; accepted 6 July 2023; published 21 July 2023)

By incorporating the quantum effects and the Coulomb interaction between the first ionized electron and the residual ion in a uniform theory, the Coulomb-corrected quantum-trajectories (CCQT) method is developed to describe the recollision-impact ionization (RII) process in nonsequential double ionization of atoms in intense laser field. The results simulated by CCQT are found to be in better agreement with the experimental results, compared with those calculated by the classical-trajectory Monte Carlo (CTMC) and strong-field approximation (SFA) methods. Considering its advantage of small computational cost and back-trajectory analysis, the CCQT method will be an efficient theoretical tool to quantitatively investigate the underlying physics of the complex and coherent multielectron dynamics in intense laser field.

DOI: 10.1103/PhysRevA.108.013115

I. INTRODUCTION

Nonsequential double ionization (NSDI) in intense laser field has attracted considerable interest (for reviews, see, e.g., Refs. [1,2]), since it was discovered 40 years ago [3], because it is regarded as one dramatic manifestation of electron-electron correlation in nature. It is commonly accepted that NSDI results from the laser-induced inelastic recollision. In the recollision process [4,5], the first electron is ionized through tunneling, then is driven back by the laser field to collide with the parent ion. If the kinetic energy of the first active electron is high enough, it releases the second electron directly (recollision-impact ionization, RII). In contrast, if the kinetic energy transferred from the first electron to the core is not sufficient to free the second electron, the second electron can be only pumped to an excited state and then be freed by the laser field at a later time (recollision excitation with subsequent ionization, RESI).

The understanding on NSDI mainly relies on four kinds of theoretical methods, all of which have their limitations. The classical (semiclassical) method in Monte Carlo frame, also known as the classical-trajectory Monte Carlo (CTMC) method, obtains electron trajectories by numerically solving Newton equations [6–9]. It takes the full interactions into account, including laser-electron, ion-electron, as well as electron-electron Coulomb interactions. But due to its classical nature, it does not include the quantum effect such as the parity of the quantum state [10,11] and the interference effect [12–16]. The quantitative rescattering (QRS) model, taking advantage of the precise differential cross section (DCS), does not include the interference effect either. Strong-field approximation (SFA) [17,18] describes the quantum effect well but ignores the Coulomb interaction between the residual ion and the freed electron, which may cause problems in the quantitative or even qualitative description of NSDI. For example, since the coulomb focusing effect on the electron trajectory is ignored, the multiple return trajectories are underestimated, and the calculated results [19] are not consistent with the experimental results at high laser intensity [20]. Numerical solution of the time-dependent Schrödinger equation (TDSE) [21,22] is the most accurate theoretical method, but to solve it is a formidable computational challenge and it is difficult to provide deep insight into the underlying mechanism. Therefore, a coherent and quantitative approach which can incorporate all the abovementioned effects in a uniform theory is highly demanded. Very recently, a Coulomb-corrected quantum-trajectories (CCQT) method [23], in which both the quantum effect and Coulomb interaction between the electron and the parent ion are considered, was proposed to investigate the RESI process. It quantitatively reproduced the experimentally observed different patterns of correlated electron momentum distributions (CEMDs) in the below-threshold laser intensity regime, and identified the key role played by the recollision of the second electron.

In this paper, the CCQT method is developed to investigate the RII process of Ne atoms. It has been confirmed that, unlike in He and Ar, the RII process plays a major role in the NSDI

*xlhao@sxu.edu.cn
†wfyang@hainanu.edu.cn
‡chen_jing@iapcm.ac.cn

of Ne [24–26]. We obtain the CEMDs for Ne at different laser wavelengthes and different laser intensities. After comparing the simulated results with the experimental results as well as with that calculated by SFA and CTMC methods, we find that better agreement is achieved between the simulated results of CCQT and the experimental results. Especially, the flaw of underestimation of multireturn trajectories in SFA is remedied in the recently developed CCQT method.

II. THEORETICAL METHODS

A. SFA

The SFA transition amplitude for the RII process in length gauge can be expressed as (atomic units $m = \hbar = e = 1$ are used) [12]

$$M(\mathbf{p}_1, \mathbf{p}_2) = \int_{-\infty}^{\infty} dt_2 \int_{-\infty}^{t_2} dt_1 \int d^3\mathbf{k} \times \langle \mathbf{p}_2+\mathbf{A}(t_2), \mathbf{p}_1+\mathbf{A}(t_2)|V_{12}|\psi_g^{(2)}, \mathbf{k}+\mathbf{A}(t_2)\rangle \times \langle \mathbf{k}+\mathbf{A}(t_1)|V_1|\psi_g^{(1)}\rangle \exp[iS(t_2, t_1, \mathbf{k})], \quad (1)$$

where $|\psi_g^{(i)}\rangle$ is the ground state of the ith electron e_i. For Ne atoms focused here, we employ the hydrogen-like wave function of the $2p$ state to describe the ground state of the two electrons with the effective nuclear charge $Z_i = \sqrt{2I_{pi}}$, where I_{pi} denotes the ionization potential of e_i for Ne. $|\mathbf{k}+\mathbf{A}(t)\rangle$ is the plane wave with momentum $\mathbf{k}+\mathbf{A}(t)$, and $\mathbf{A}(t)$ is the vector potential. In the calculation of this work, a linearly polarized plane-wave laser field with $\mathbf{A}(t) = A_0 \cos \omega t$ (ω corresponds to the frequency of 800-nm or 1300-nm laser field) is applied. V_1 denotes the binding potential of e_1, and V_{12} is the interaction between the two electrons. t_1 is the ionization time and t_2 is the rescattering time of e_1. The action S is expressed as

$$S(t_2, t_1, \mathbf{k}) = -\int_{t_2}^{\infty} \frac{[\mathbf{p}_1+\mathbf{A}(\tau)]^2}{2} d\tau - \int_{t_2}^{\infty} \frac{[\mathbf{p}_2+\mathbf{A}(\tau)]^2}{2} d\tau - \int_{t_1}^{t_2} \frac{[\mathbf{k}+\mathbf{A}(\tau)]^2}{2} d\tau + I_{p1}t_1 + I_{p2}t_2. \quad (2)$$

The infinite upper limit of the first two integrals in the above action is immaterial. It introduces a phase that cancels when calculating the probabilities, and therefore does not contribute to any observable.

The multiple integrals in Eq. (1) can be solved using saddle-point methods:

$$M(\mathbf{p}_1, \mathbf{p}_2) = \sum_s \frac{(2\pi i)^{5/2}}{\sqrt{\det S''(t_2, t_1, \mathbf{k})|_s}} \times \langle \mathbf{p}_2+\mathbf{A}(t_2^s), \mathbf{p}_1+\mathbf{A}(t_2^s)|V_{12}|\psi_g^{(2)}, \mathbf{k}^s+\mathbf{A}(t_2^s)\rangle \times \langle \mathbf{k}^s+\mathbf{A}(t_1^s)|V_1|\psi_g^{(1)}\rangle \exp[iS(t_2^s, t_1^s, \mathbf{k}^s)], \quad (3)$$

where the index s runs over the relevant saddle points and $S''(t_2, t_1, \mathbf{k})|_s$ denotes the five-dimensional matrix of the second derivatives to the action in Eq. (2) with respect to $t_1, t_2, \mathbf{k}$. The corresponding saddle-point equations are

$$[\mathbf{k}+\mathbf{A}(t_1)]^2 = -2I_{p1}, \quad (4)$$

$$[\mathbf{p}_1+\mathbf{A}(t_2)]^2 + [\mathbf{p}_2+\mathbf{A}(t_2)]^2 = [\mathbf{k}+\mathbf{A}(t_2)]^2 - 2I_{p2}, \quad (5)$$

$$\int_{t_1}^{t_2} d\tau [\mathbf{k}+\mathbf{A}(\tau)] = 0. \quad (6)$$

B. CCQT method

Following the same idea of the CCQT method for RESI process [23], the ionization and propagation of e_1 are calculated by employing the quantum trajectory Monte Carlo (QTMC) method [27,28] to include the effect of the Coulomb interaction between the residual ion and the first ionized electron. And the inelastic recollision process resulting in double ionization (DI) is calculated by conventional SFA. Then, the magnitude of the RII process in length gauge can be expressed as

$$M(\mathbf{p}_1, \mathbf{p}_2) = \sum_s M^{(2)}_{\mathbf{p}_1,\mathbf{p}_2}(t_2^s) M^{(1)}_{\widetilde{\mathbf{k}}}(t_2^s, t_1^s). \quad (7)$$

The above magnitude is summed over different trajectories s, and t_1^s and t_2^s denote the ionization time and rescattering time of the first electron for trajectory s.

$M^{(1)}_{\widetilde{\mathbf{k}}}(t_2, t_1)$ describes the ionization process of e_1 and its propagation in the combined laser field and electron-core Coulomb field by employing the QTMC method,

$$M^{(1)}_{\widetilde{\mathbf{k}}}(t_2, t_1) = \sqrt{w(t_1)} \exp[iS_1(t_2, t_1)], \quad (8)$$

where $w(t_1)$ is the tunneling ionization rate calculated with the Ammosov-Delone-Krainov formula [29], which is determined by the instantaneous laser electric field at the ionization time t_1. The classical action S_1 in Eq. (8) is expressed as

$$S_1(t_2, t_1) = -\int_{t_1}^{t_2} \left[\frac{\widetilde{\mathbf{v}}_1^2(\tau)}{2} - \frac{1}{|\mathbf{r}_1(\tau)|} \right] d\tau + I_{p1}t_1, \quad (9)$$

where $\widetilde{\mathbf{v}}_1(t)$ is the instantaneous velocity of e_1, which is obtained by solving the Newton equation $d\widetilde{\mathbf{v}}_1(t)/dt = -\mathbf{E}(t) - \mathbf{r}_1(t)/|\mathbf{r}_1(t)|^3$ with $\mathbf{E}(t) = -\partial\mathbf{A}(t)/\partial t$. After being ionized at time t_1 through tunneling, e_1 propagates in the combined field of the Coulomb potential and the laser field until it collides with the ion at time t_2 when the distance between e_1 and the ion reaches a minimum.

$M^{(2)}_{\mathbf{p}_1,\mathbf{p}_2}(t_2)$ describes the DI process at time t_2

$$M^{(2)}_{\mathbf{p}_1,\mathbf{p}_2}(t_2) = \langle \mathbf{p}_2+\mathbf{A}(t_2), \mathbf{p}_1+\mathbf{A}(t_2)|V_{12}|\psi_g^{(2)}, \widetilde{\mathbf{k}}+\mathbf{A}(t_2)\rangle \times \exp[iS_2(t_2)]. \quad (10)$$

This term is similar to the first term in the integral in Eq. (1) except that the undisturbed intermediate asymptotic momentum $\mathbf{k}$ is replaced with Coulomb-field disturbed intermediate asymptotic momentum $\widetilde{\mathbf{k}} = \widetilde{\mathbf{v}}_1(t) - \mathbf{A}(t)$. The excess energy after overcoming I_{p2} is randomly allocated to the two electrons, only to ensure the energy conservation $[\mathbf{p}_1+\mathbf{A}(t_2)]^2/2 + [\mathbf{p}_2+\mathbf{A}(t_2)]^2/2 = [\widetilde{\mathbf{k}}+\mathbf{A}(t_2)]^2/2 - I_{p2}$ similar to the saddle-point equation Eq. (5). The directions of $\mathbf{p}_1$ and $\mathbf{p}_2$ are chosen randomly. The classical action S_2 in

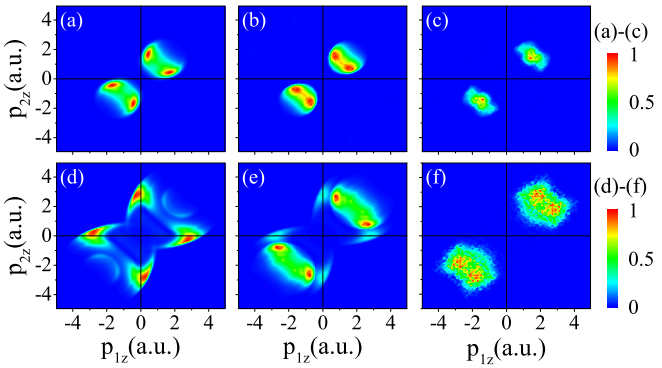

FIG. 1. CEMDs for Ne atoms with the same laser parameters as the experimental results in Fig. 3 of Ref. [26]. [(a)–(c)] 800 nm, 3×10^{14}W/cm^2, corresponding to ponderomotive energy $U_p = 0.656$ a.u.; [(d)–(f)] 1300 nm, 2.6×10^{14} W/cm^2, corresponding to ponderomotive energy $U_p = 1.502$ a.u. (a) and (d) are calculated with the SFA method, (b) and (e) are calculated with the CCQT method, and (c) and (f) are calculated with the CTMC method.

Eq. (10) is expressed as

$$S_2(t_2) = -\int_{t_2}^{\infty} \frac{[\mathbf{p}_1+\mathbf{A}(\tau)]^2}{2} d\tau - \int_{t_2}^{\infty} \frac{[\mathbf{p}_2+\mathbf{A}(\tau)]^2}{2} d\tau + I_{p2} t_2. \tag{11}$$

In general, the main difference between the SFA model and the CCQT model comes from the treatment of the propagation of the first electron before recollision. In the SFA model, the quantum trajectories are obtained by solving the saddle-point equations, i.e., Eqs. (4)–(6). In these equations, the Coulomb interaction between the residual ion and the first ionized electron is ignored, whereas in the CCQT model we calculate these rescattering trajectories by including the Coulomb interaction. This improvement will correct the momentum of the first electron, its classical action (phase), and also the probability of recollision, and eventually influence the NSDI process.

C. CTMC method

In the CTMC method [6], e_1 is firstly tunnel ionized at the outer edge of the laser-field suppressed Coulomb potential. The initial tunnel exit, the initial transverse velocity, and the weight of each electron trajectory are calculated according to the adiabatic tunneling theory [29]. After ionization, the evolution of e_1 is governed by the three-dimensional (3D) Newton equations of motion. The bound electron e_2 is assumed to be in the ground state of Ne^+, and its initial distribution is simulated by a microcanonical distribution [30]. To mimic the RII process, we only take into account trajectories with delay time—interval between recollision time and double ionization time—smaller than $0.1T$ (T is the optical cycle). In our calculation, a laser pulse of six cycles with constant amplitude plus three cycles of ramp down is applied.

III. RESULTS AND DISCUSSION

Figure 1 displays the simulated CEMDs for Ne atoms at wavelengthes of 800 nm and 1300 nm to compare with the high-resolution experimental results in Fig. 3 of Ref. [26]. The laser parameters in our calculations are the same as those in the experiments. At a wavelength of 800 nm, CEMDs calculated with three methods all concentrate in the first and third quadrants, indicating that the two electrons prefer to emit in the same direction. A V-shape structure can be seen clearly in the SFA and CCQT results [Figs. 1(a) and 1(b)], but is not obvious in the CTMC result [Fig. 1(c)]. The V-shape structure in the CCQT result is narrower than that in the case of SFA, and is more consistent with the experimental result in Ref. [26]. At a wavelength of 1300 nm, the SFA result tilts to the second and fourth quadrants [Fig. 1(d)], while for CCQT and CTMC, distributions in the first and third quadrants are always dominant, which is also the case for the experimental results. Compared to the CTMC result, the V structure in the CEMD of CCQT is wider, and is closer to the axis. In addition, two additional parts of distribution appear along the axis in the result of CCQT. Actually, on close inspection of the experimental result at 1300 nm (Fig. 3(b) in Ref. [26]), one can find a similar pattern including both the wider V structure and the additional distribution near the axis. In general, among the three theoretical methods, CCQT results show better agreement with the experimental results at both wavelengthes.

In addition, the authors of Ref. [26] also presented simulated results of the SFA model, which are in good agreement with their experimental results. Their SFA model is quite different from the one applied in this work. First, the two-electron final state in Ref. [26] involves the Coulomb repulsion of the two electrons, which is neglected in the product of two independent one-electron Volkov state employed in this work. However, we apply the pure Coulomb repulsive potential as the electron-electron interaction V_{12} in the transition amplitude, which is responsible for the ionization of the second electron at the rescattering. In Ref. [26], the authors employed the Yukawa potential V_{12} with a free parameter of the effective screening factor. For the value of the effective screening factor selected in Ref. [26], the effect of the long-range Coulomb interaction is actually not included. In short, the Coulomb repulsion of the two electrons is considered in both SFA models but in different ways. In Ref. [26], the Coulomb repulsion of the two electrons is taken into account in the final two-electron state, but is not fully considered in the interaction potential V_{12}. In contrast, in our SFA model, it is not included in our final state, but is fully considered in the interaction potential V_{12}. It is worth noting that the pattern of the momentum distribution is sensitive to the effective screen factor if employing a Yukawa potential, so an appropriate value of this parameter is critical to obtain consistent results with the experiment. Moreover, the authors of Ref. [26] only considered the first-return rescattering trajectories in their calculations, whereas in our calculation, besides the first-return trajectories, we also include multireturn trajectories which will be found to have important contribution.

We also compare the simulated results of three methods for different laser intensities at a wavelength of 800 nm. When laser intensity increases, all distributions calculated by the three methods become wider. From 5×10^{14} W/cm^2, the SFA-calculated CEMD [Fig. 2(a)] tends to be more and more inconsistent with the CCQT and CTMC results [Figs. 2(b) and 2(c)]. The SFA result tilts to and finally concentrates in

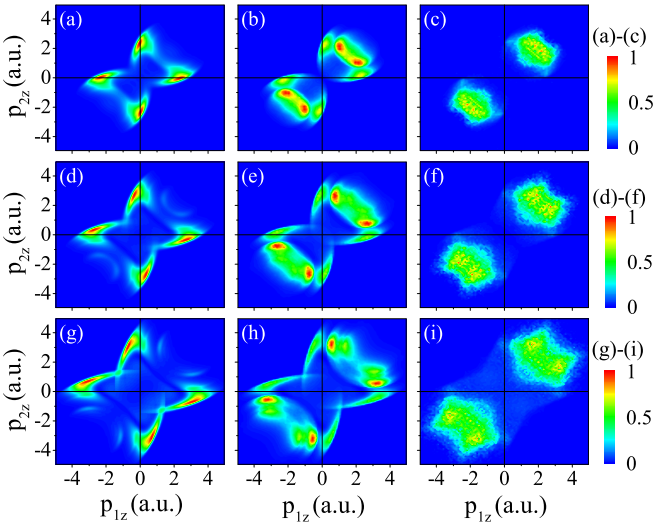

FIG. 2. CEMDs for Ne atoms at 800 nm for different laser intensities. [(a)–(c)] 5×10^{14} W/cm^2; [(d)–(f)] 7×10^{14} W/cm^2, and [(g)–(i)] 1×10^{15} W/cm^2. (a), (d), and (g) are calculated with the SFA method; (b), (e), and (h) are calculated with the CCQT method; and (c), (f), and (i) are calculated with the CTMC method. All CEMDs are normalized to themselves.

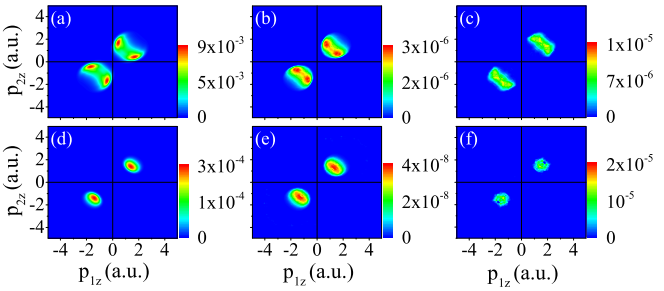

FIG. 3. CEMDs for different-return trajectories at 3×10^{14} W/cm^2. [(a)–(c)] The first-return trajectory. [(d)–(f)] The third-return trajectory. (a) and (d) are calculated with the SFA method. (b) and (e) are calculated with the CCQT method. (c) and (f) are calculated with the CTMC method.

the second and fourth quadrants [see Figs. 2(d) and 2(g)]. For CCQT and CTMC, although distributions tend to be visible in the second and fourth quadrants when laser intensity increases, distributions in the first and third quadrants are always dominant [see Figs. 2(h) and 2(i)], which are qualitatively consistent with the experimental results at 1×10^{15} W/cm^2 [20]. In addition, there exists a quantitative difference between CCQT and CTMC results. Compared with CTMC, the V-shape structure in CEMD of CCQT is wider, and the distribution in the second and fourth quadrants is more prominent. It is worth noting that CEMDs at 7×10^{14} W/cm^2 [Figs. 2(d)–2(f)] are unsurprisingly consistent with the results at 1300 nm in Fig. 2 since they have nearly equal ponderomotive potential $U_p = E^2/4\omega^2$ (E is the laser electric field and ω is the angular frequency).

It has been demonstrated that the deviation of SFA results from CTMC results at large U_p can be attributed to the underestimation of the multireturn trajectories due to the ignorance of the Coulomb interaction between e_1 and the residual ion in SFA [19]. Here, the main correction made in the CCQT model is including the electron-core Coulomb field during the propagation of e_1 before recollision; this is why the CCQT results exhibit better agreement with the experimental results than the results calculated with the SFA model. If the electron-core Coulomb interaction is ignored, the diffusion effect will cause smaller probability of rescattering trajectories with longer travel time Δt (the interval between the ionization time t_1 and the recollision time t_2). So the contribution of the multireturn trajectories ($\Delta t > T$, T is the optical period) is much lower than that of the first-return trajectories ($\Delta t < T$) in the results of SFA. However, if the electron-core Coulomb interaction is considered, just as is done in the CCQT model, the Coulomb focusing effect will compensate the diffusion effect, and the probability of multireturn trajectories will be significantly improved. Since the momentum distribution of multireturn trajectories is different from that of the first-return trajectories, the increase of the contribution of the multireturn trajectories leads to the change of the shape of the final momentum distribution, which is found to be in better agreement with the experimental results. Next, we will make a detailed analysis of the contributions of different-return trajectories to further demonstrate the above explanation. Here, different-return trajectories of e_1 are defined according to the travel time Δt. For trajectories with Δt in the interval $[(n/2)T, ((n+1)/2)T]$, we denote them as the nth-return trajectories [31]. To show the case clearly, we separate the contributions of different-return trajectories to CEMDs at 800 nm obtained by three theoretical methods, respectively.

At the lowest laser intensity of 3×10^{14} W/cm^2, the maximal return energy of the first-return trajectory is well above the ionization potential I_{p2}, and that of the third-return trajectory is slightly higher than I_{p2}. The maximal energy of the second-return trajectory is insufficient to ionize e_2, so it does not contribute to NSDI. In Fig. 3 we present CEMDs for the first- and third-return trajectories at 3×10^{14} W/cm^2. The patterns of CEMD calculated by the three methods are qualitatively consistent with each other. The first-return trajectory exhibits a clear V-shape structure, whereas the distribution of the third-return trajectory is much narrower and concentrates on the diagonal, which is resulted from the much smaller excess energy of the third-return trajectory after overcoming I_{p2}. Quantitatively, the yield of the third-return trajectory is much lower than that of the first return in the results of CCQT and SFA, but the yields of the first and the third return are comparable in CTMC results. Since the distribution region of the first- and third-return trajectories overlap each other, the V-shape structure in the total CEMD of CTMC [Fig. 1(c)] becomes not obvious.

When laser intensity increases to 5×10^{14} W/cm^2, distribution of the first return tilts to the axis of $p_z = 0$ in all three cases [see Fig. 4]. Such laser-intensity dependence can be easily understood. The final momenta of the two electrons are determined by the residual momenta after inelastic recollision and momenta obtained by them from the laser field after recollision, which is equal to $-\mathbf{A}(t_2)$. The residual momentum and the laser-induced momentum $-\mathbf{A}(t_2)$ are in opposite directions in forward scattering, which is the main

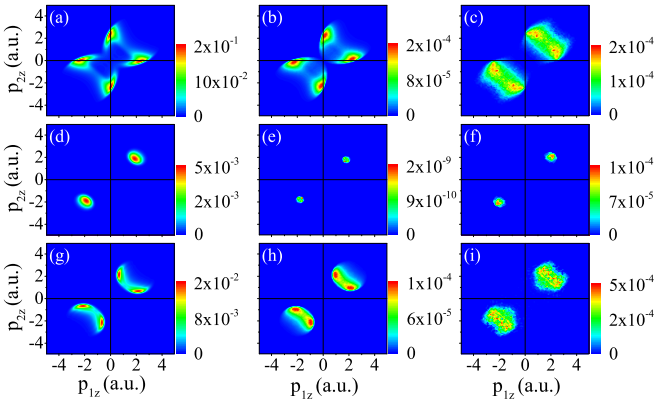

FIG. 4. CEMDs for different-return trajectories at 5×10^{14} W/cm^2. [(a)–(c)] The first-return trajectory. [(d)–(f)] The second-return trajectory. [(g)–(i)] The third-return trajectory. (a), (d), and (g) are calculated with the SFA method. (b), (e), and (h) are calculated with the CCQT method. (c), (f), and (i) are calculated with the CTMC method.

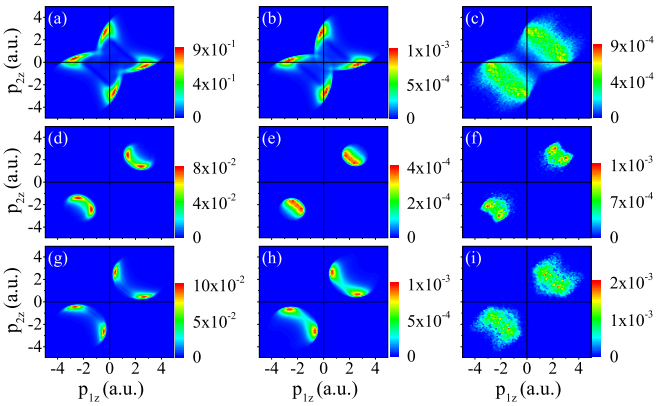

FIG. 5. CEMDs for different-return trajectories at 7×10^{14} W/cm^2. [(a)–(c)] The first-return trajectory. [(d)–(f)] The second-return trajectory. [(g)–(i)] The third-return trajectory. (a), (d), and (g) are calculated with the SFA method. (b), (e), and (h) are calculated with the CCQT method. (c), (f), and (i) are calculated with the CTMC method.

case in the present situation. At lower intensity, the value of $-\mathbf{A}(t_2)$ is higher, so the final momenta is in the direction of the laser-induced momentum. With increasing laser intensity, the residual momentum increases faster than $-\mathbf{A}(t_2)$. Therefore, the momenta of the electrons become smaller, i.e., the distribution tilts to the axis. For the second-return trajectory, its maximal return energy is just above I_{p2} at this intensity, so it begins to contribute to NSDI. Similar to the third-return trajectory at 3×10^{14} W/cm^2, the excess energy for the second return here is very small, so its distribution is very narrow and concentrates on the diagonal. For the third-return trajectory, the higher excess energy allows a V-shape structure to appear. All patterns of distribution are similar among the three methods, but the relative contributions of different-return trajectories are different. For CTMC and CCQT, the relative contribution of the third return increases compared with the first return, whereas for SFA, it nearly has no change.

As the laser intensity further increases, evolution of the CEMDs for different-return trajectories proceeds (see Figs. 5 and 6). Distribution of the first-return trajectory shifts to the second and fourth quadrants. The V-shape structure begins to form in the CEMD of the second return, and that of the third return becomes wider and gradually approaches the axis. Since the first-return trajectory always contributes dominantly in the case of SFA, the total CEMDs behave like the first-return trajectory. For CTMC, the third-return trajectory plays a dominant role, so the total CEMDs mainly distribute in the first and third quadrants. In CCQT results, the contribution of the third-return trajectory is comparable to that of the first return, so the pattern of the total CEMD is somewhere between the other two methods. The maxima of the distribution are in the first and third quadrants, while at the same time, distribution in the second and fourth quadrants is also visible. This is the case in Figs. 2(e) and 2(h), and is also the case in Fig. 1(e), which is consistent with the experimental result.

In Fig. 7 we present the laser-intensity dependence of the proportions of different-return trajectories. For SFA [Fig. 7(a)], the proportions for different-return trajectories almost have no change. The contributions of the second- and third-return trajectories are always one order magnitude lower than the first return. The results of CCQT [Fig. 7(b)] and CTMC [Fig. 7(c)] show similar trends: the proportion of the first return decreases monotonously, the second return increases monotonously, while the third return first increases and then decreases slightly. However, a quantitative difference between the results of these two methods can be found. The proportion for the third return of CTMC exceeds that of the first return, but the third return is always lower than the first return in CCQT results. This difference can be attributed to the fact that, in the CCQT method, the quantum cross section of double ionization in Eq. (10) only depends on the energy of the incident particles, and is independent of the impact parameter. In contrast, in the classical treatment, the cross section of double ionization is sensitive to the impact parameter. The smaller the impact parameter, the higher the cross section.

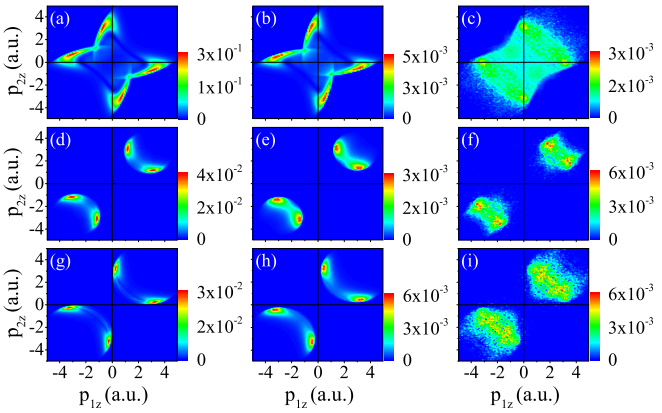

FIG. 6. CEMDs for different-return trajectories at 1×10^{15} W/cm^2. [(a)–(c)] The first-return trajectory. [(d)–(f)] The second-return trajectory. [(g)–(i)] The third-return trajectory. (a), (d), and (g) are calculated with the SFA method. (b), (e), and (h) are calculated with the CCQT method. (c), (f), and (i) are calculated with the CTMC method.

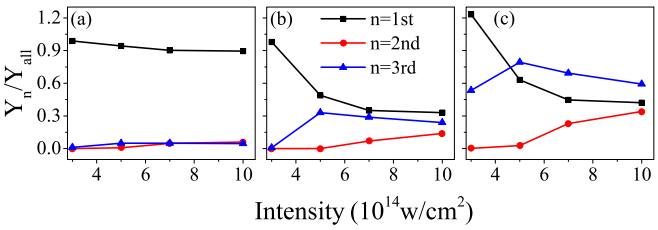

FIG. 7. The contribution rate of different returns to the total CEMD with the laser intensity. (a) The SFA method. (b) The CCQT method. (c) The CTMC method.

It has been reported that the third-return trajectories show a much narrower distribution of impact parameter than the first-return trajectories [31]. As a result, the relative contribution of the third-return trajectories in CTMC is higher than that in CCQT. Therefore, it seems that the contribution of third-return trajectories is somewhat overestimated in the CTMC method.

In conclusion, we develop the CCQT method, in which both the quantum effect and the Coulomb interaction between the electron and the parent ion are considered, to investigate the RII process. Using this method, we calculate the CEMDs of Ne atoms for different laser parameters, which are in better agreement with the experimental results compared with that simulated by SFA and CTMC methods. Analysis shows that the flaw of underestimation of the multireturn trajectories is remedied in the CCQT method. It is noted that although the interference effect is not obvious in the present results, under what condition it will be prominent is no doubt an intriguing problem which should be explored.

ACKNOWLEDGMENTS

This work was partially supported by the National Key Research and Development Program of China (Grant No. 2019YFA0307700) and the National Natural Science Foundation of China (Grants No. 12274273, No. 91950101, and No. 12147215.

[1] A. Becker, R. Dörner, and R. Moshammer, Multiple fragmentation of atoms in femtosecond laser pulses, J. Phys. B: At. Mol. Opt. Phys. **38**, S753 (2005).

[2] W. Becker, X. J. Liu, P. J. Ho, and J. H. Eberly, Theories of photoelectron correlation in laser-driven multiple atomic ionization, Rev. Mod. Phys. **84**, 1011 (2012).

[3] A. L'Huillier, L. A. Lompre, G. Mainfray, and C. Manus, Multiply Charged Ions Formed by Multiphoton Absorption Processes in the Continuum, Phys. Rev. Lett. **48**, 1814 (1982).

[4] K. J. Schafer, Baorui Yang, L. F. DiMauro, and K. C. Kulander, Above Threshold Ionization Beyond the High Harmonic Cutoff, Phys. Rev. Lett. **70**, 1599 (1993).

[5] P. B. Corkum, A Plasma Perspective on Strong-Field Multiphoton Ionization, Phys. Rev. Lett. **71**, 1994 (1993).

[6] J. Chen, J. Liu, L. B. Fu, and W. M. Zheng, Interpretation of momentum distribution of recoil ions from laser-induced nonsequential double ionization by semiclassical rescattering model, Phys. Rev. A **63**, 011404(R) (2000).

[7] P. J. Ho, R. Panfili, S. L. Haan, and J. H. M. Eberly, Nonsequential Double Ionization as a Completely Classical Photoelectric Effect, Phys. Rev. Lett. **94**, 093002 (2005).

[8] X. L. Hao, G. Q. Wang, X. Y. Jia, W. D. Li, J. Liu, and J. Chen, Nonsequential double ionization of Ne in an elliptically polarized intense laser field, Phys. Rev. A **80**, 023408 (2009).

[9] L. Sarkadi, Laser-induced nonsequential double ionization of helium: Classical model calculations, J. Phys. B: At. Mol. Opt. Phys. **53**, 165401 (2020).

[10] C. Li, J. Liu, X. L. Hao, X. Y. Jia, W. D. Li, and J. Chen, Ionic-state-resolved electron–electron correlation in strong-field double ionization, Results Phys. **29**, 104647 (2021).

[11] C. Li, X. L. Hao, X. Y. Jia, W. D. Li, and J. Chen, Intensity dependence of ionic-state-resolved electron-electron correlation in strong-field double ionization, Phys. Scr. **96**, 125403 (2021).

[12] S. V. Popruzhenko, Ph. A. Korneev, S. P. Goreslavski, and W. Becker, Laser-Induced Recollision Phenomena: Interference Resonances at Channel Closings, Phys. Rev. Lett. **89**, 023001 (2002).

[13] X. L. Hao, J. Chen, W. D. Li, B. Wang, X. Wang, and W. Becker, Quantum Effects in Double Ionization of Argon below the Threshold Intensity, Phys. Rev. Lett. **112**, 073002 (2014).

[14] A. S. Maxwell and C. Figueira de Morisson Faria, Controlling Below-Threshold Nonsequential Double Ionization via Quantum Interference, Phys. Rev. Lett. **116**, 143001 (2016).

[15] W. Quan, X. L. Hao, Y. L. Wang, Y. J. Chen, S. G. Yu, S. P. Xu, Z. L. Xiao, R. P. Sun, X. Y. Lai, S. L. Hu, M. Q. Liu, Z. Shu, X. D. Wang, W. D. Li, W. Becker, X. J. Liu, and J. Chen, Quantum interference in laser-induced nonsequential double ionization, Phys. Rev. A **96**, 032511 (2017).

[16] M. Waitz, D. Metz, J. Lower, C. Schober, M. Keiling, M. Pitzer, K. Mertens, M. Martins, J. Viefhaus, S. Klumpp, T. Weber, H. Schmidt-Böcking, L. Ph. H. Schmidt, F. Morales, S. Miyabe, T. N. Rescigno, C. W. McCurdy, F. Martín, J. W. Williams, M. S. Schöffler, T. Jahnke *et al.*, Two-Particle Interference of Electron Pairs on a Molecular Level, Phys. Rev. Lett. **117**, 083002 (2016).

[17] R. Kopold, W. Becker, H. Rottke, and W. Sandner, Routes to Nonsequential Double Ionization, Phys. Rev. Lett. **85**, 3781 (2000).

[18] A. Becker and F. H. M. Faisal, Interpretation of Momentum Distribution of Recoil Ions from Laser Induced Nonsequential Double Ionization, Phys. Rev. Lett. **84**, 3546 (2000).

[19] X. Y. Jia, X. L. Hao, D. H. Fan, W. D. Li, and J. Chen, S-matrix and semiclassical study of electron-electron correlation in strong-field nonsequential double ionization of Ne, Phys. Rev. A **88**, 033402 (2013).

[20] R. Moshammer, J. Ullrich, B. Feuerstein, D. Fischer, A. Dorn, C. D. Schroter, J. R. Crespo Lopez-Urrutia, C. Hohr, H. Rottke, C. Trump, M. Wittmann, G. Korn, K. Hoffmann, and W. Sandner, Strongly directed electron emission in non-sequential double ionization of Ne by intense laser pulses, J. Phys. B: At. Mol. Opt. Phys. **36**, L113 (2003).

[21] J. S. Parker, L. R. Moore, K. J. Meharg, D. Dundas, and K. T. Taylor, Double-electron above threshold ionization of helium, J. Phys. B: At. Mol. Opt. Phys. **34**, L69 (2001).

[22] S. G. Chen, W. C. Jiang, S. Grundmann, F. Trinter, M. S. Schöffler, T. Jahnke, R. Dörner, H. Liang, M. X. Wang, L. Y. Peng, and Q. H. Gong, Photon Momentum Transfer in Single-Photon Double Ionization of Helium, Phys. Rev. Lett. **124**, 043201 (2020).

[23] X. L. Hao, Y. X. Bai, C. Li, J. Y. Zhang, W. D. Li, W. F. Yang, M. Q. Liu, and J. Chen, Recollision of excited electron in below-threshold nonsequential double ionization, Commun. Phys. **5**, 31 (2022).

[24] V. L. B. de Jesus, B. Feuerstein, K. Zrost, D. Fischer, A. Rudenko, F. Afaneh, C. D. Schroter, R. Moshammer, and J. Ullrich, Atomic structure dependence of nonsequential double ionization of He, Ne and Ar in strong laser pulses, J. Phys. B: At. Mol. Opt. Phys. **37**, L161 (2004).

[25] Z. J. Chen, Y. Q. Liang, D. H. Madison, and C. D. Lin, Strong-field nonsequential double ionization of Ar and Ne, Phys. Rev. A **84**, 023414 (2011).

[26] T. Shaaran, N. Camus, J. Dura, L. Fechner, A. Thai, A. Britz, M. Baudisch, T. Steinle, A. Senftleben, C. D. Schröter, J. Ullrich, T. Pfeifer, C. H. Keitel, J. Biegert, K. Z. Hatsagortsyan, and R. Moshammer, Role of high ponderomotive energy in laser-induced nonsequential double ionization, Phys. Rev. A **99**, 023421 (2019).

[27] M. Li, J. Geng, H. Liu, Y. Deng, C. Wu, L. Peng, Q. Gong, and Y. Liu, Classical-Quantum Correspondence for Above-Threshold Ionization, Phys. Rev. Lett. **112**, 113002 (2014).

[28] X. Song, C. Lin, Z. Sheng, P. Liu, Z. Chen, W. Yang, S. Hu, C. D. Lin, and J. Chen, Unraveling nonadiabatic ionization and Coulomb potential effect in strong-field photoelectron holography, Sci. Rep. **6**, 28392 (2016).

[29] N. B. Delone and V. P. Krainov, Energy and angular electron spectra for the tunnel ionization of atoms by strong low-frequency radiation, J. Opt. Soc. Am. B **8**, 1207 (1991).

[30] J. S. Cohen, Comment on the classical-trajectory Monte Carlo method for ion-atom collisions, Phys. Rev. A **26**, 3008 (1982).

[31] X. L. Hao, Y. X. Bai, X. Y. Zhao, C. Li, J. Y. Zhang, J. L. Wang, W. D. Li, C. L. Wang, W. Quan, X. J. Liu, Z. Shu, M. Liu, and J. Chen, Effect of Coulomb field on laser-induced ultrafast imaging methods, Phys. Rev. A **101**, 051401(R) (2020).